Arch. Min. Sci. **69** (2024), 4, 615-632

Electronic version (in color) of this paper is available: http://mining.archives.pl

DOI: https://doi.org/10.24425/ams.2024.152577

ANTONI TAJDUŚ[1], JERZY FLISIAK[1], KRZYSZTOF TAJDUŚ[2*]

NUMERICAL INSIGHTS INTO STRESS CHANGES INDUCED BY LONGWALL MINING IN FAULTED ROCK MASSES

Conducting mining operations in fault zones is a very challenging task, both from a technological perspective and also due to the safety of the miners. Therefore, it is essential to determine the impact of mining parameters on the possibility of fault activation, which in many cases leads to high seismic activity. The article presents the results of numerical analyses of the impact of longwall mining in the vicinity of tectonic faults on the state of stress in the rock masses. The authors demonstrated the influence of the advancement of the longwall face and its direction on the risk of rock burst, both for mining conducted in the footwall and hanging wall.

Keywords: Rock burst; faults; longwall mining; seismic events; stress; friction coefficient

1. Introduction

The exploitation of coal deposits triggers seismic activity in the rock mass, manifesting as tremors, including highly dangerous high-energy tremors with energy exceeding 10^7 J. Seismic events of such high energies often do not cause damage in the mine workings but are strongly felt on the surface as vibrations, frequently leading to damage to buildings [1-4].

One of the most significant factors causing the occurrence of high-energy tremors is the presence of faults and their activation during mining activities in their vicinity. This issue applies not only to underground exploitation of solid deposits [5-7], but also to other forms of mining activities, such as the exploitation of fluid deposits [8,9], hydraulic fracturing [10,11], under-

[1] AGH UNIVERSITY OF KRAKOW, AL. MICKIEWICZA 30, 30-059 KRAKOW, POLAND
[2] STRATA MECHANICS RESEARCH INSTITUTE, POLISH ACADEMY OF SCIENCES, 27 REYMONTA STR., 30-059, KRAKÓW, POLAND

* Corresponding author: tajdus@imgpan.pl

ground energy storage [12-15] CO_2 sequestration [16,17], or the construction and exploitation of geothermal deposits [10,18,19].

From the authors' experiences and analyses of scientific publications, it is evident that the mere presence of a fault leads to significant disturbances in the original stress state, the degree of which depends on the conditions prevailing on the fault surface and increases with a decrease in the friction coefficient.

In the study by Tajduś et al. [20], numerical calculations were performed for 256 cases involving normal faults with varying inclinations (γ) and rock deformation parameters: Young's modulus (E) and Poisson's ratio (ν). As a result, the critical value of the friction coefficient (μ_{cr}) was determined, above which no displacement occurs on the fault. The critical value of the friction coefficient can be determined from the relationship (with a correlation coefficient of 0.995):

$$\mu_{cr} = \frac{1}{\tan\tan\gamma}\left[\frac{0.0128 \cdot E + 1.221}{\nu} - 1.935\right] \tag{1}$$

If the friction coefficient value $\mu > \mu_{cr}$, then there is no displacement on the fault. However, when $\mu \leq \mu_{cr}$ conditions exist for sudden displacement on the fault during longwall mining, which can lead to high-energy events. The inclination angles of most faults where high-energy tremors occur range from 65° to 78°. Assuming a Young's modulus value of $E = 2.0$ GPa and a Poisson's ratio of $\nu = 0.3$ for coal, critical friction coefficient values fall within the range $0.5 < \mu_{cr} < 1.0$. Therefore, an increase in the fault inclination angle γ from 65° to 78° results in a decrease in the critical friction coefficient value. Laboratory studies by Byerlee [21] indicate that the friction coefficient on the fault is approximately $\mu = 0.85$.

2. Mining of coal seams in the vicinity of faults

Mining conducted in areas with faults causes a change in the stress state, the magnitude of which depends on:

- the location of the longwall panels in the fault area:
  - mining is conducted in the footwall of the fault,
  - mining is conducted in the hanging wall of the fault,
- the orientation of the longwall panel relative to the fault:
  - mining is conducted parallel to the fault,
  - mining is conducted perpendicular to the fault,
- the distance between the exploited longwall panel and the fault.

In order to evaluate the influence of faults on mining operations nearby, a three-dimensional numerical model was developed, representing common conditions observed in coal mines in Poland. Within the central portion of the model (see Fig. 1), spanning 6,000 m in length, 1,000 m in width, and 1,200 m in height, a plane depicting a normal fault with an inclination of 2.5:1.0 ($\gamma = 68.20°$) and a throw of 55 m was located, with frictional forces present on its surface.

It is assumed that in the hanging wall, a coal seam with a thickness of 4.0 m is located at a depth of $H = 700$ m ($\sigma_z = 17.5$ MPa). Directly above it lies a layer of sandy shale with a thickness of 16 m, above which is a layer of strong sandstone with a thickness of 30 m. It is assumed that the rocks forming the rock mass behave elastically, and their properties are as follows:

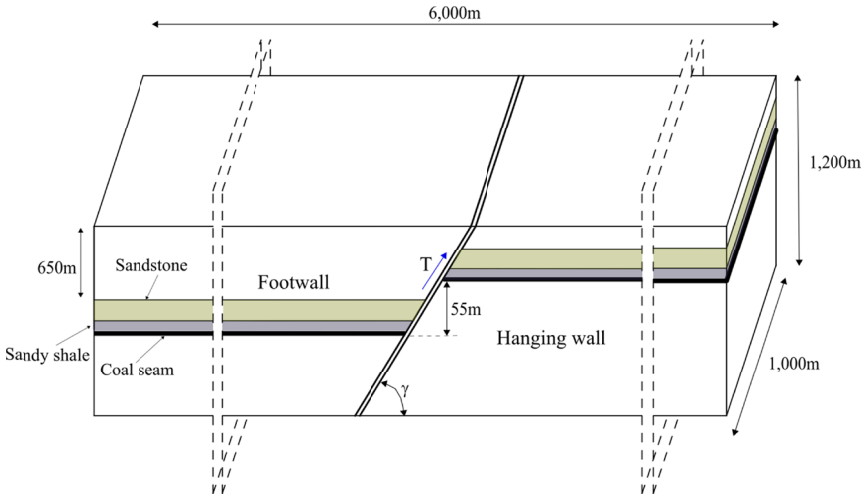

Fig. 1. Diagram of the numerical model used for calculations

TABLE 1

Mechanical parameters of the rock layers adopted for calculations

Layer	Young's Modulus E [GPa]	Poisson's Ratio ν	Density ρ [kg/m^3]	Strength [MPa]	
				R_c	R_r
Sandy shale	5.0	0.25	2,500	40	4.0
Coal	2.0	0.30	1,600	28	2.5
Sandstone	15.0	0.12	2,500	70	7.0
Caved zone	0.2	0.40	2,100	—	—
Fracture zone	0.5	0.35	2,300	—	—

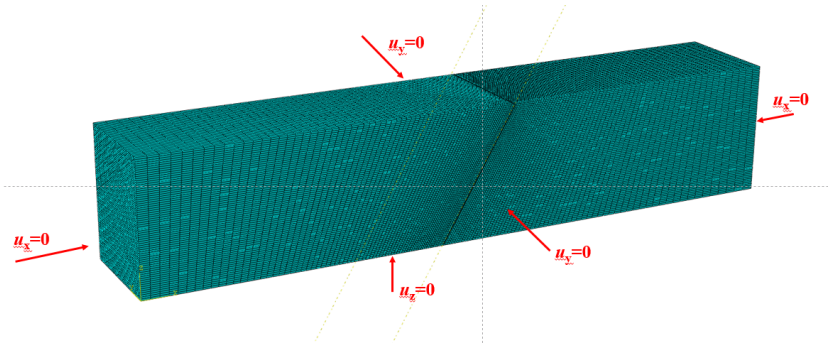

Fig. 2. Sample of the meshed model with boundary conditions

The general appearance of the numerical model is presented in Fig. 2. The entire model consisted of approximately 1,400,000 hexahedral elements. Boundary conditions related to the

restriction of node displacements in specific directions were applied to the individual external surfaces of the model (Fig. 2). The model allowed the nodes to move in the remaining directions not marked in Fig. 2.

The model itself consisted of two parts connected by contact. The contact surface simulated a fault, and its characteristics (friction coefficient, inclination angle) varied for different calculation variants. An initial stress state was applied to the model at the outset, which changed as the exploitation progressed. The exploitation of the longwall system with roof fall was simulated by removing elements in the working space and altering the deformation properties of elements in the fall zone and fractured zone, according to the data provided in TABLE 1 and the methodology described in the article [22].

Rockburst is an energetic phenomenon. The energetic changes occurring in the rock mass can be generally described by Eq. (2) [23]. The left side of this equation defines the energy delivered to the part of the rock mass involved in the rockburst process, with its rocks undergoing destruction, mainly brittle. On the right side of the equation, energies determining the consequences of the rockburst are present.

$$\phi_n + \phi_d = L_{zn} + \phi_k + \phi_s + \phi_r \tag{2}$$

where:

- ϕ_d – additional energy initiating rockburst supplied from the outside (this could be energy resulting from sudden collapse of thick, strong rock layers, e.g., sandstone, or displacement on a fault),
- L_{zn} – work expended on rock destruction in the volume of rock mass involved in the rockburst process (part of the rocks are thrown into the workings),
- ϕ_k – kinetic energy of the destroyed rocks (its value determines the consequences of the rockburst),
- ϕ_s – seismic energy (measured by seismic instruments – seismometers),
- ϕ_r – dissipated energy (which is consumed by plastic deformations, thermal effects, acoustic effects, etc.),
- ϕ_n – elastic energy accumulated in the part of the rock mass that undergoes destruction during the rockburst.

The value of energy ϕ_n is the sum of the primary elastic energy existing in the rock mass before mining initiation ϕ_p, and the elastic energy generated as a result of mining activities ϕ_e is:

$$\phi_n = \phi_p + \phi_e \tag{3}$$

Of the four types of energy on the right side of Eq. (2) determining the consequences of the rockburst, the values of the first two are primarily decisive: the energy converted into work, which is expended on the destruction of a specific part of the rock mass L_{zn}, and the kinetic energy ϕ_k, which determines the strength of the rockburst. Together ($L_{zn} + \phi_k$) absorb about 90% of the elastic energy accumulated in the rock mass region participating in the rockburst. This is due, among other things, to the fact that the value of seismic energy ϕ_s is nearly two orders of magnitude smaller than the energy released at the rockburst source [23]. Taking this into account, Eq. (2) can be simplified as:

$$(\phi_n + \phi_d) \cdot 0.9 = L_{zn} + \phi_k \tag{4}$$

The magnitude of the energy expended on rock destruction can be estimated using criteria of failure. Roughly, we can use the Huber-Mises-Hencky criterion, which is based on the magnitude of the strain energy, or more precisely, Burzyński's strength criterion. In Burzyński's criterion, it is assumed that the destruction of material in a complex stress and strain state is determined by the total value of strain energy and a certain portion of volumetric strain energy.

In this article, the energy expended on destruction was estimated using the Huber-Mises-Hencky criterion. It is assumed that at the moment of destruction, the strain energy ϕ_f is converted into the work of rock structure destruction L_{zn}, i.e.:

$$\phi_f = L_{zn} \tag{5}$$

Assuming the deformation and strength data from TABLE 1, from Eq. (5), it can be estimated that the critical value of energy at which coal destruction occurs is approximately $L_{zn} = 0.7 \times 10^5$ J/m^3.

The kinetic energy ϕ_k can be estimated using the formula:

$$\phi_k = \frac{1}{2}\rho V_p^2 \tag{6}$$

where:

ρ – the average density of the part of the rock mass that has been destroyed (from TABLE 2),

V_p – the average initial velocity of rocks from the damaged zone. According to Pietuchow [24], this velocity ranges from 3.0 to 10.6 m/s, while from the authors' experience, it averages around 10 m/s. Of course, in the case of strong rockbursts, this energy is often much higher.

Assuming the averaged value ρ for the surrounding rocks of the mined panel $\rho = 2.4 \times 10^3$ kg/m^3, and $V_p = 10.0$ m/s, the estimated value of kinetic energy will be: $\phi_k^{sr} = 1.2 \times 10^5$ J/m^3.

TABLE 2

Example average density values of rocks (own research)

Rock layer	**ρ [kg/m^3]**
Shale	2.4×10^3
Sandy shale	2.2×10^3
Sandstone	2.6×10^3
Coal	1.6×10^3

The value of kinetic energy strongly depends on the value of volumetric energy ϕ_o. Taking into account the above considerations as well as previous experiences, three indicators were adopted to assess the risk of rockbursts in the fault zone:

The value of kinetic energy strongly depends on the volumetric energy value ϕ_o. Considering the above discussions as well as previous experiences, three indicators were adopted to assess the rockburst hazard in the fault area:

- The first indicator determines the ratio of the larger, compressive principal stress σ_2 to the initial vertical stress p_z: $\alpha = \dfrac{\sigma_2}{p_z}$,

- The second indicator is the density of elastic strain energy, which is a measure of the energy required to destroy rock, calculated by the formula:

$$\phi_f = \frac{1}{12G}\left[(\sigma_1-\sigma_2)^2+(\sigma_2-\sigma_3)^2+(\sigma_3-\sigma_1)^2\right] \tag{7}$$

- The third indicator, defined by the density of elastic strain energy of volumetric deformation, is a measure of the kinetic energy that can be released during a rockburst:

$$\phi_o = \frac{1}{18K}(\sigma_1+\sigma_2+\sigma_3)^2 \tag{8}$$

where:

$$G = \frac{E}{2(1+\nu)},$$

$$K = \frac{E}{3(1-2\nu)}.$$

2.1. Longwall mining conducted towards the fault in the footwall

The aim of the research discussed in this section was to determine changes in stress state and assess the degree of rockburst risk as the wall face approaches the fault in the footwall (Fig. 3) using the finite element method.

TABLE 3 provides extreme values of principal stresses in the roof of the seam, $\sigma_1 \geq \sigma_3 \geq \sigma_2$, for two values of the friction coefficient on the fault: $\mu = 1.0$, $\mu = 0.5$. For comparison, calculations were made for the maximum values of principal stresses and strain energies (both post-strain and volumetric) in the roof of the mined longwall panel in the absence of a fault (under the same

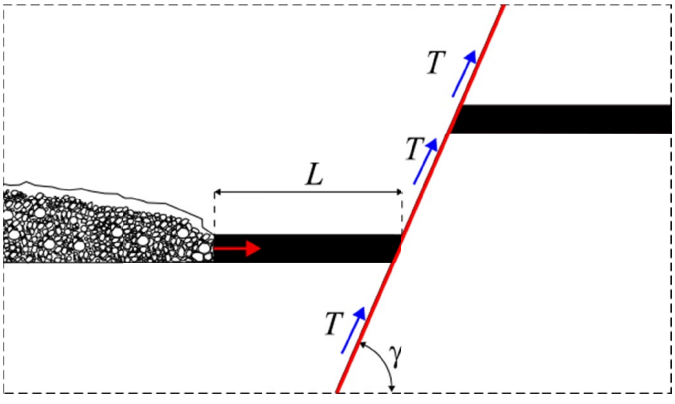

Fig. 3. Schematic overview of the numerical model aimed at assessing the risk of rockbursts as the wall face approaches the fault in the footwall

remaining mining-geological conditions). The calculations yielded the following maximum values of principal stresses and rockburst risk indicators:

$$\sigma_1 = -18.6 \text{ [MPa]}, \sigma_2 = -43.8 \text{ [MPa]}, \alpha = 2.5,$$
$$\phi_f = 1.1\times10^5 \text{ [J/m}^3\text{]}, \phi_o = 1.8\times10^5 \text{ [J/m}^3\text{]}.$$

TABLE 3

Change in maximum values of principal stresses and rockburst risk indicators: α, ϕ_f and ϕ_o in the roof of the seam with distance L [m] to the fault, for two values of the friction coefficient on the fault: $\mu = 1.0$, $\mu = 0.5$

L [m]	Friction coefficient $\mu = 1.0$					Friction coefficient $\mu = 0.5$				
	σ_1 [MPa]	σ_2 [MPa]	α	$\phi_f\times10^5$ [J/m^3]	$\phi_o\times10^5$ [J/m^3]	σ_1 [MPa]	σ_2 [MPa]	α	$\phi_f\times10^5$ [J/m^3]	$\phi_o\times10^5$ [J/m^3]
200	–17.9	–44.8	2.6	1.2	1.8	–16.2	–47.7	2.7	1.6	1.8
120	–17.9	–44.8	2.6	1.2	1.8	–16.2	–47.7	2.7	1.6	1.8
80	–17.9	–44.8	2.6	1.2	1.8	–16.3	–47.7	2.7	1.6	1.8
40	–18.3	–46.3	2.7	1.3	1.9	–16.3	–49.0	2.8	1.7	1.9
30	–19.5	–47.9	2.8	1.4	2.0	–16.6	–51.4	2.9	1.9	2.1
15	–20.3	–51.0	2.9	1.6	2.3	–17.1	–54.8	3.1	2.4	2.3
8	–21.8	–58.9	3.4	2.2	2.9	–18.1	–61.1	3.5	2.8	2.8

In TABLE 4, extreme values of principal stresses in the base of the sandstone layer, located 30 m above the coal seam, are provided for two values of the friction coefficient on the fault: $\mu = 1.0$, $\mu = 0.5$.

TABLE 4

Change in maximum values of principal stresses and rockburst risk indicators: α, ϕ_f and ϕ_o with distance L [m] from the fault in the base of the sandstone layer, for two values of the friction coefficient on the fault: $\mu = 1.0$, $\mu = 0.5$

L [m]	Friction coefficient $\mu = 1.0$					Friction coefficient $\mu = 0.5$				
	σ_1 [MPa]	σ_2 [MPa]	α	$\phi_f\times10^5$ [J/m^3]	$\phi_o\times10^5$ [J/m^3]	σ_1 [MPa]	σ_2 [MPa]	α	$\phi_f\times10^5$ [J/m^3]	$\phi_o\times10^5$ [J/m^3]
200	–7.3	–28.4	1.7	0.7	0.6	–7.7	–29.5	1.7	0.7	0.6
120	–7.4	–28.4	1.7	0.7	0.6	–7.8	–29.6	1.7	0.7	0.6
80	–7.4	–28.4	1.7	0.7	0.6	–7.8	–29.7	1.7	0.7	0.6
40	–7.4	–28.5	1.7	0.7	0.6	–7.8	–29.8	1.8	0.7	0.6
30	–7.5	–31.5	1.8	0.9	0.7	–7.8	–32.7	1.9	0.9	0.7
15	–7.5	–34.4	2.0	1.1	0.8	–7.9	–36.9	2.2	1.2	0.9
8	–7.5	–36.3	2.1	1.2	0.9	–7.9	–40.8	2.4	1.6	1.1

The change in maximum values of normal stresses and shear stresses on the fault as the wall approaches the fault is shown in TABLE 5.

TABLE 5

Change in maximum values of normal and shear stresses on the fault as the longwall face approaches the fault

L [m]	Maximum stresses on the fault plane				
	Numerical calculation		Limit shear stress for the friction coefficients $\tau_{gr} = \sigma_n \cdot \mu$ [MPa]		
	Stress				
	Normal σ_n^{max} [MPa]	Shear τ_s^{max} [MPa]	$\mu = 0.5$	$\mu = 0.85$	$\mu = 1.0$
200	6.0	3.0	3.0	5.1	6.0
80	9.5	4.0	4.8	8.1	9.5
40	11.5	5.5	5.8	9.8	11.5
30	12.5	6.0	6.3	10.7	12.5
15	13.5	7.0	6.8	11.5	13.5

The calculations presented above indicated several important dependencies. Firstly, it was observed that as the mining face approaches the fault, the maximum values of normal and shear stresses on the fault increase (TABLE 5). With a friction coefficient on the fault close to $\mu = 0.5$, there is a high probability of movement on the fault as the value of shear stresses on the fault approaches or exceeds the shear strength, even at a distance of 15 m from the fault. The estimated inclinations of most faults near which high-energy tremors occur are in the range of $65° < \gamma < 78°$. For a fault inclination angle $\alpha = 65°$ the critical value of the friction coefficient is $\mu_{kr} = 1.0$, meaning that when the friction coefficient is less than 1.0, sudden displacement on the fault can occur. An increase in the fault inclination angle from 65° to 78° results in a decrease in the critical value of the friction coefficient to $\mu_{kr} = 0.5$ (halved). The magnitude of stress changes depends on the friction coefficient on the fault. The lower the friction on the fault, the higher the values of maximum compressive stresses in its vicinity. It was also noted that as the mining face approaches the fault, compressive stresses increase, and the risk of rockburst increases as measured by the value of strain energy (both post-strain and volumetric). Comparing the obtained stress values for cases with and without a fault (taking $\alpha = 2.75$ as a critical value), the values of obtained post-strain and volumetric energies can be estimated as follows:

- for a friction coefficient on the fault $\mu = 1.0$, the minimum safe distance of the wall face from the fault is 35 m,
- for a friction coefficient on the fault $\mu = 0.5$, the safe distance of the wall face from the fault is 55 m.

It was also observed that approximately 15% lower stress values are obtained in the base of the sandstone located 30 m above the seam.

2.2. Longwall mining conducted away from the fault in the footwall

The aim of the subsequent numerical calculations was to determine changes in stress state and assess the degree of rockburst risk as the wall face moves away from the fault in the footwall. TABLE 6 provides the maximum values of principal stresses in the roof of the seam, $\sigma_1 \geq \sigma_3 \geq \sigma_2$ for a friction coefficient on the fault of $\mu = 1.0$.

TABLE 6

Extreme values of stress tensor components and rockburst risk indicators: α, ϕ_f and ϕ_o in the roof of the seam and in the base of the sandstone during longwall panel advance away from the fault

L [m]	Values of stress tensor components [MPa]									
	In a seam roof					In a sandstone floor				
	σ_1 [MPa]	σ_2 [MPa]	α	$\phi_f \times 10^5$ [J/m^3]	$\phi_o \times 10^5$ [J/m^3]	σ_1 [MPa]	σ_2 [MPa]	α	$\phi_f \times 10^5$ [J/m^3]	$\phi_o \times 10^5$ [J/m^3]
8	–7.6	–26.7	1.5	0.6	0.5	–6.2	–19.8	1.2	0.3	0.3
15	–8.3	–27.1	1.6	0.6	0.6	–6.3	–22.4	1.4	0.4	0.3
30	–9.1	30.3	1.8	0.7	0.7	–6.4	–24.3	1.5	0.5	0.4
40	–9.7	–32.3	1.9	0.8	0.8	–6.5	–27.5	1.7	0.7	0.6
80	–10.8	–37.6	2.1	1.1	1.0	–7.7	–32.6	2.0	0.9	0.8
120	–11.2	–40.7	2.3	1.3	1.2	–8.3	–36.4	2.2	1.1	0.9
200	–11.4	–44.4	2.5	1.6	1.4	–9.0	–38.6	2.4	1.3	1.0

Typically, mining is conducted within a maximum distance of 30 m from the fault (both when the longwall face approaches the fault and when starting progress away from the fault). Therefore, at a distance of 30 m from the fault, extreme stress values and adopted rockburst risk indicators obtained for mining towards the fault and away from the fault were compared.

TABLE 7

Comparison of mining conducted away from the fault with mining conducted towards the fault

Operation conducted in the direction: (for boundary L = 30 m)	Stress tensor components [MPa]									
	In the roof of the seam					In the floor of the sandstone layer				
	σ_1	σ_2	α	$\phi_f \times 10^5$ [J/m^3]	$\phi_o \times 10^5$ [J/m^3]	σ_1	σ_2	α	$\phi_f \times 10^5$ [J/m^3]	$\phi_o \times 10^5$ [J/m^3]
from the fault	–9.7	–32.3	1.9	0.7	0.7	–6.5	–27.5	1.7	0.5	0.4
to the fault	–18.3	–46.3	2.7	1.4	2.0	–7.5	–31.5	1.8	0.9	0.7

Based on the conducted numerical calculations, it has been observed that longwall mining of the coal seam in the direction away from the fault is significantly more favourable than towards the fault. This is indicated by the stress values as well as the values of potential and volumetric energy occurring both in the exploited wall and in the bottom of the sandstone layer. This observation pertains to changes in the stress state within the rock mass in the immediate vicinity of the mining operation. However, it should be noted that research related to the occurrence of discontinuous deformations in fault areas unequivocally indicates a significant increase in the risk of discontinuous deformation when mining is conducted towards the fault. Results of analyses conducted for 1,138 registered discontinuities in the Ruhr District [25] area have shown that the probability of discontinuous deformation occurring significantly increases when mining moves away from the fault. This is related to the horizontal tensile deformations occurring in the rock mass (+).

2.3. Longwall mining conducted towards the fault in the hanging wall

From mining experience as well as numerical analyses, it is evident that the degree of stress disturbance caused by the existence of a fault in the hanging wall is significantly smaller than in the footwall. Therefore, the conditions for conducting mining in the hanging wall should be more favourable compared to mining in the footwall. To investigate this issue, calculations were conducted where longwall mining was modelled in a manner analogous to the description above. Numerical calculations were performed for different distances of the mining face from the fault, starting mining 200 m away from the fault and gradually approaching it (see Fig. 4). It was assumed that there is friction on the fault surface with a coefficient of $\mu = 1.0$. Calculations conducted for lower friction coefficient values are qualitatively similar, although the degree of disturbance is greater. TABLE 8 presents the results obtained from the numerical calculations.

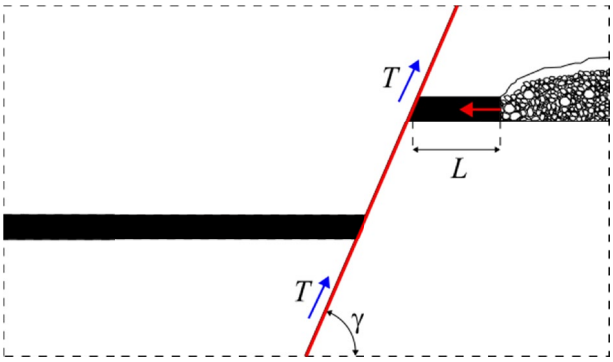

Fig. 4. Schematic diagram of the numerical model aimed at assessing the risk of roof rock burst as the face approaches the fault in the hanging wall

TABLE 8

Extreme values of stress tensor components and collapse hazard indicators: α, ϕ_f and ϕ_o in the roof of the seam and in the sandstone floor as longwall mining approaches the fault in the hanging wall

L [m]	Stress tensor components [MPa]									
	In the roof of the seam					In the roof of the seam				
	σ_1 [MPa]	σ_2 [MPa]	α	$\phi_f \times 10^5$ [J/m^3]	$\phi_o \times 10^5$ [J/m^3]	σ_1 [MPa]	σ_2 [MPa]	α	$\phi_f \times 10^5$ [J/m^3]	$\phi_o \times 10^5$ [J/m^3]
200	–11.0	–36.6	2.1	1.0	1.0	–7.4	–28.0	1.7	0.6	0.6
120	–11.4	–38.7	2.1	1.1	1.1	–7.5	–28.3	1.7	0.6	0.6
80	–11.7	–38.6	2.2	1.1	1.1	–7.6	–28.4	1.7	0.6	0.6
40	–12.0	–38.8	2.3	1.1	1.2	–8.0	–28.6	1.8	0.6	0.6
30	–12.8	–40.6	2.4	1.2	1.3	–8.1	–30.8	1.9	0.8	0.7
15	–14.1	–44.2	2.6	1.4	1.5	–8.2	–34.0	2.1	1.0	0.8
8	–14.6	–58.4	3.4	2.9	2.4	–10.4	–48.0	2.9	2.1	1.5

In TABLE 9, a comparison of the obtained calculation results is presented for mining conducted towards the fault in the footwall and mining conducted in the hanging wall, with a boundary distance from the fault equal to $L = 30$ m

TABLE 9

Comparison of longwall mining conducted towards the fault in the footwall with longwall mining conducted in the hanging wall for a distance of $L = 30$ m from the fault

Exploitation towards the fault	Stress tensor components [MPa]									
	In the roof of the seam					In the roof of the seam				
	σ_1	σ_2	α	$\phi_f \times 10^5$ [J/m^3]	$\phi_o \times 10^5$ [J/m^3]	σ_1	σ_2	α	$\phi_f \times 10^5$ [J/m^3]	$\phi_o \times 10^5$ [J/m^3]
In the footwall	–19.5	–47.9	2.8	1.4	2.0	–7.5	–31.5	1.8	0.9	0.7
In the hanging wall	–12.8	–40.6	2.4	1.2	1.3	–8.1	–30.8	1.9	0.8	0.7

Based on the obtained results, the following conclusions regarding mining in the hanging wall were formulated:

- Similar to mining in the footwall, as the mining face approaches the fault, the absolute stress values increase. Up to a distance of about 30 m from the fault, the rate of stress increase is small. At distances less than 30 m from the fault, there is an intense increase in stress tensor components as well as potential and volumetric energy.
- A comparison of calculation results for mining in the hanging wall and footwall indicates that in footwall mining, the absolute values of principal stresses, as well as energies ϕ_f and ϕ_o, reach significantly higher values. This suggests that mining in the hanging wall occurs under more favourable conditions in terms of collapse hazard. Despite similar values of potential energy (which mainly determines rock failure), volumetric energy, influencing collapse energy, increases significantly (by about 35%).
- From the authors' experience and numerical analyses (not included in the paper), it is evident that mining coal in rock masses with higher strength and deformation parameters than those considered leads to even greater collapse hazards.

2.4. Longwall mining conducted parallel to the fault

The analysis focused on longwall mining of a 200 m length face along the fault. Numerical calculations were conducted for three variants:

- Mining at a distance of 40 m from the fault,
- Mining at a distance of 20 m from the fault,
- Mining at a distance of 5 m from the fault.

It was assumed that the mining is conducted in the footwall, with segments every 100 m (see Fig. 5). TABLES 10 and 11 provide the change in maximum principal stress values along with the advancement of panel exploitation and indicators determining the risk of tremors and the possibility of rock burst. TABLE 10 presents the results for the wall conducted along the fault at a distance of 40 m from the fault, while TABLE 11 presents the results at a distance of 5 m from the fault. Stress values and indicators determining the collapse hazard are given for the sandstone floor located 20 m above the exploited longwall panel.

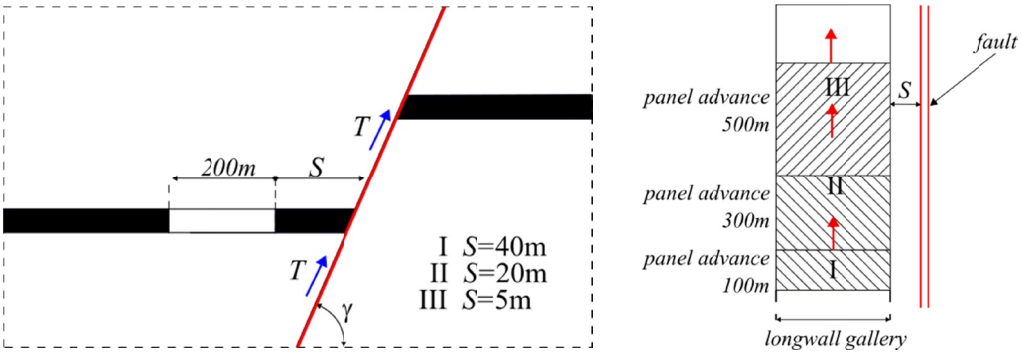

Fig. 5. Schematic diagram of the numerical model aimed at assessing the risk of rock burst for longwall mining along the fault

TABLE 12 shows the change in maximum normal and shear stress values on the fault as the face moves along the fault.

TABLE 10

Maximum principal stress values and indicators determining the risk of tremors and rock burst for the panel conducted along the fault at a distance of 40 m from the fault

Face advance L [m]	**Exploitation at a distance of 40 m from the fault**						
	σ_1^{max} [MPa]	σ_2^{max} [MPa]	α	$\phi_f \times 10^5$ [J/m^3]	$\phi_o \times 10^5$ [J/m^3]	σ_n^{max} [MPa]	τ_s^{max} [MPa]
100	–5.7	–27.2	1.7	0.7	0.5	12.8	5.1
300	–6.7	–30.8	2.0	0.8	0.6	13.9	5.8
500	–6.8	–32.4	2.1	0.9	0.7	14.2	6.0

TABLE 11

Maximum principal stress values and indicators determining the risk of tremors and rock burst for the panel conducted along the fault at a distance of 5 m from the fault

Face advance L [m]	**Exploitation at a distance of 5 m from the fault**						
	σ_1^{max} [MPa]	σ_2^{max} [MPa]	α	$\phi_f \times 10^5$ [J/m^3]	$\phi_o \times 10^5$ [J/m^3]	σ_n^{max} [MPa]	τ_s^{max} [MPa]
100 m	–5.8	–28.5	1.8	0.8	0.5	15.8	9.0
300 m	–6.7	–33.5	2.1	1.0	0.7	18.6	11.2
500 m	–6.9	–34.6	2.2	1.1	0.8	19.1	11.6

From TABLE 12, it can be observed that as the mining face moves along the fault, the maximum normal and shear stress values on the fault increase. The greatest changes occur in the range from 100 m to 300 m of the face advance. With a friction coefficient on the fault close to $\mu = 0.5$, there is a high probability of movement on the fault. When the wall conducted along the fault is at a distance $S \leq 20$ m from it, the shear stresses on the fault are greater than the shear strength.

TABLE 12

Change in maximum normal and shear stress values on the fault as the face moves along the fault

Distance from the fault (S)	L [m]	Maximum stresses on the fault plane				
		Numerical calculation		Friction: $\tau_{gr} = \sigma_n \cdot \mu$ [MPa] for		
		Stress				
		Normal σ_n^{max} [MPa]	Shear τ_s^{max} [MPa]	$\mu = 0.5$	$\mu = 0.85$	$\mu = 1.0$
40 m	100	12.8	5.1	6.4	10.9	12.8
	300	13.9	5.8	7.0	11.8	13.9
	500	14.2	6.0	7.1	12.1	14.2
5 m	100	15.8	9.0	7.9	13.4	15.8
	300	18.6	11.2	9.3	15.8	18.6
	500	19.1	11.6	9.6	16.2	19.1

In TABLE 13, a comparison is made between the results of maximum principal stresses and indicators determining the risk of tremors and rock burst for the longwall conducted along the fault at a distance of 40 m from it, with the results obtained for the same distance in the case of mining towards the fault.

TABLE 13

Comparison of maximum principal stress values and indicators determining the risk of tremors and rock burst for the panel conducted along the fault at a distance of 40 m from it, with the results obtained for the same distance in the case of mining towards the fault

Exploitation in the footwall	At the floor of the sandstone layer, 40 m away from the fault				
	σ_1	σ_2	α	$\phi_f \times 10^5$ [J/m^3]	$\phi_o \times 10^5$ [J/m^3]
Towards the fault	–7.4	–28.5	1.7	0.7	0.6
Along the fault	–6.9	–34.6	2.2	1.1	0.8

Based on the obtained results and their analysis, the following conclusions have been formulated:

- During exploitation parallel to the fault, stresses and indicators determining the risk of tremors and rock burst increase as the face advances. Stress concentrations approach maximum values already after the wall has been exploited for approximately 300 m. This result is consistent with observations in mining conditions, as after exploiting approximately 300 m, the number of tremors significantly increases. The maximum vertical stress value is about 20% higher after exploiting a 500 m wall compared to after exploiting a 100 m wall,
- As the width of the pillar between the exploited face and the fault decreases, there is a noticeable increase in stress concentrations on the fault surface, both shear and normal stresses. Very high shear stress gradients and high stress values on the fault indicate serious stability threats for the wall conducted at a distance of less than 40 m from the fault.

It is surprising that reducing the distance from the fault from 40 m to 5 m does not result in a significant increase in stresses or potential and volumetric energies,
- Maximum compressive stress values during exploitation along the fault are over 20% higher than those obtained when the face approaches the fault perpendicularly,
- Uneven loading along the length of the wall, particularly greater from the fault side, must be considered during the exploitation of the wall parallel to the fault.

3. Examples from mining observations of conducting longwall panels near faults

3.1. The influence of distance from the fault on the quantity and energy of tremors during longwall mining in the footwall along the fault

Analysing the impact of distance from the fault on the quantity and energy of tremors during longwall mining in the footwall along the fault, an analysis was conducted on three walls with an average length of 240 m and heights ranging from 3.8 m to 4.1 m, conducted along the fault. The fault had an inclination of $\alpha = 68°$ and a throw of 40m. The exploited walls were at different distances from the fault, with the average depth of the exploited walls being 640 m. During the mining of these walls, tremors of varying quantity and energy were observed, ranging from 10^3 J to even 10^9 J. The tremors were divided into three energy intervals:
- tremors of moderate energy from the range of 10^3 to 10^4 J,
- tremors of high energy from the range of 10^5 to 10^6 J,
- tremors of very high energy from the range of 10^7 to 10^9 J (also called regional tremors).

The number of tremors is given in parentheses (see TABLE 14).

TABLE 14

Change in tremor energy with increasing distance from the fault

Longwall	The distance of the wall face from the fault	The total energy of tremors, in selected intervals [J] (number of tremors in parentheses)			The total energy [J]
		$10^3 \div 10^4$	$10^5 \div 10^6$	$10^7 \div 10^9$	
1	35 m	1.4×10^7 (797)	0.4×10^8 (111)	2.57×10^9 (5)	2.62×10^9 (913)
2	255 m	1.8×10^7 (771)	2.2×10^8 (227)	0	2.38×10^8 (998)
3	475 m	2.0×10^7 (879)	1.7×10^8 (171)	0.03×10^9 (1)	2.16×10^8 (1051)

From the analysis of TABLE 14, it can be concluded that as the distance of the wall conducted along the fault from the fault increases, there is a decrease in the number of tremors with very high energy in the range of 10^7 to 10^9 J, while the number of tremors with moderate ($10^3 \div 10^4$ J) and high energy ($10^5 \div 10^6$ J) increases. This is more favourable in terms of collapse hazard.

3.2. Change in tremor energy with increasing face advance

An analysis was conducted on the change in tremor energy with increasing face advance of longwall panel No. 2 (moving away from the starting point of wall 2, see Fig. 6). The analysis revealed that the total tremor energy increases with the advancement of the face, reaching a maximum value of (4.75×10^7) and then gradually decreasing. In the face advance from 110 m to 300 m, the energy is higher than 3.0×10^7 (see TABLE 15, Fig. 7). This section of the longwall face is particularly hazardous in terms of rock burst (Fig. 7).

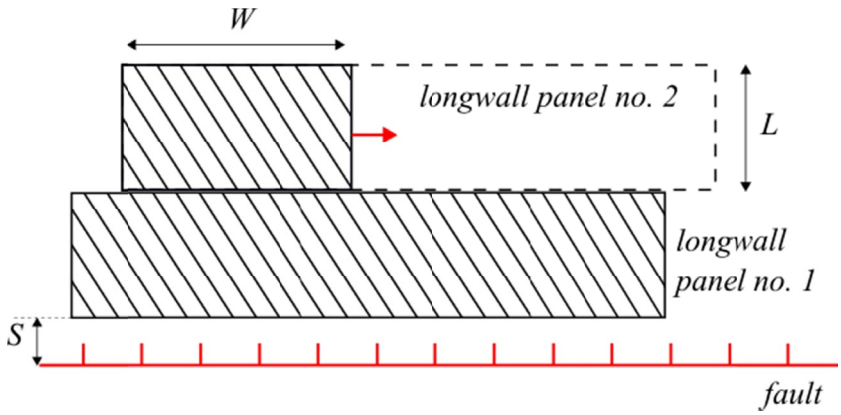

Fig. 6. Schematic diagram of the numerical model of mining along the fault

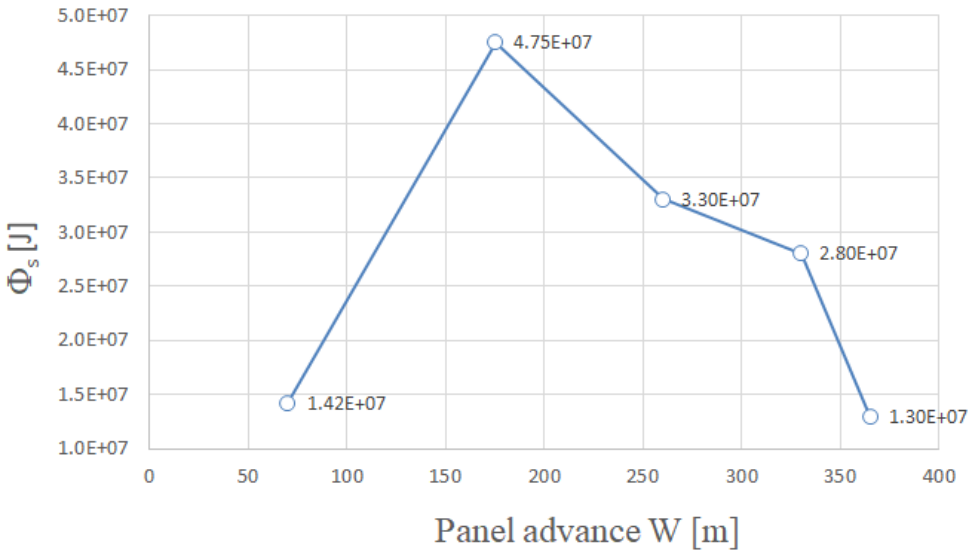

Fig. 7. The values of tremor energy for longwall panel no. 2

TABLE 15

Changes in tremor energy with the advancement of longwall panel no. 2.

Panel advance no. 2	Total tremor energy [J], in respective intervals				Sum of seismic events	Total energy [J]
	10^3	10^4	10^5	10^6		
70	56	18	3	3	80	1.42×10^7
175	46	42	19	13	119	4.75×10^7
260	106	35	18	12	171	3.30×10^7
330	54	40	11	9	114	2.80×10^7
365	32	12	13	6	62	1.30×10^7

4. Discussion

Table 16 provides guidelines for selecting the dimensions of a safe pillar between the fault and the exploited wall in conditions of collapse hazard. Due to the collapse hazard, the remaining pillar between the exploited wall and the fault should not be narrower than the widths given in TABLE 16.

TABLE 16

Selection of a safe pillar between the fault and the exploited wall

Method of longwall mining	Average slope of the fault (γ)	Critical friction coefficient on the fault	Safe pillar between the fault and the exploited wall (s)
Mining in the throw side towards the fault	$\gamma \approx 65°$	$\mu_{kr} = 1.00$	35 m
	$\gamma \approx 69°$	$\mu_{kr} = 0.85$	40 m
	$\gamma \approx 78°$	$\mu_{kr} = 0.50$	55 m
Mining in the throw side away from the fault	$\gamma \approx 65°$	$\mu_{kr} = 1.00$	25 m
	$\gamma \approx 69°$	$\mu_{kr} = 0.85$	30 m
	$\gamma \approx 78°$	$\mu_{kr} = 0.50$	35 m
Mining in the hanging wall towards the fault	$\gamma \approx 65°$	$\mu_{kr} = 1.00$	30 m
	$\gamma \approx 69°$	$\mu_{kr} = 0.85$	35 m
	$\gamma \approx 78°$	$\mu_{kr} = 0.5$	45 m
Mining in the footwall along the fault	$\gamma \approx 65°$	$\mu_{kr} = 1.0$	30 m
	$\gamma \approx 69°$	$\mu_{kr} = 0.85$	35 m
	$\gamma \approx 78°$	$\mu_{kr} = 0.5$	45 m

5. Summary

Mining operations in fault zones present technological and safety challenges, requiring an understanding of the impact of mining parameters on fault activation and the associated seismic risk. Numerical analyses have shown that the advancement and direction of the mining face affect the risk of rock burst, differing based on whether the mining is conducted in the footwall or hanging wall. The study results confirmed significant changes in the stress state of rock masses,

increasing the risk of destabilisation. The authors recommend that the pillar between the mined wall and the fault should not be narrower than the widths specified in TABLE 16, minimising the risk of rock burst. The results can be used to develop guidelines for safe mining operations in fault zones, significantly enhancing work safety through proper planning of protective pillar dimensions and optimization of the mining face advancement. The article provides valuable insights into the impact of longwall mining on stress changes in rock masses and offers practical guidelines to improve miner safety.

Acknowledgements

We would like to sincerely thank Dr. Michał Kowalski from AGH for granting permission to use a portion of the numerical calculation results he conducted in the FLAC3D software in this article.

References

[1] J. Rusek, Procedure of building and analysis of information database on mining tremors of existing bridge structures. Geomatics and Environmental Engineering (2018).

[2] J. Dubiński, G. Mutke, J. Chodacki, Distribution of Peak Ground Vibration Caused by Mining Induced Seismic Events in the Upper Silesian Coal Basin in Poland. Archives of Mining Sciences **65** (3), 419-32 (2020).

[3] M. Fragiacomo, C. Amadio, L. Macorini, Seismic response of steel frames under repeated earthquake ground motions. Eng. Struct. (2004).

[4] H. Bilgin, Effects of near-fault and far-fault ground motions on nonlinear dynamic response and seismic damage of masonry structures. Eng. Struct. 300, 117200, Feb. (2024).

[5] G.F. Hofmann, L.J. Scheepers, Simulating fault slip areas of mining induced seismic tremors using static boundary element numerical modelling. Transactions of the Institutions of Mining and Metallurgy, Section A: Mining Technology **120** (1), 53-64 (2011).

[6] Z. Burtan, Conditions of fault activation in the area of conditions of fault activation in the area of exploitation. 2018 (January 2012).

[7] P.L. Swanson, Mining-induced Seismicity in Faulted Geologic Structures: An Analysis of Seismicity-induced Slip Potential. Pageoph. **139** (3) (1992).

[8] J. Rutqvist, A.P. Rinaldi, F. Cappa, P. Jeanne, A. Mazzoldi, L. Urpi, et al., Fault activation and induced seismicity in geological carbon storage – Lessons learned from recent modeling studies. Journal of Rock Mechanics and Geotechnical Engineering **8** (6), 789-804 (2016).

[9] L. Buijze, P.A.J. Van Den Bogert, B.B.T. Wassing, B. Orlic, J. Ten Veen, Fault reactivation mechanisms and dynamic rupture modelling of depletion-induced seismic events in a Rotliegend gas reservoir. Geologie en Mijnbouw/ Netherlands Journal of Geosciences **96** (5), 131-48 (2017).

[10] Z. Niu, S. Wang, H. Ma, H. Luan, Z. Ding, Study of Characteristics of Fault Slip and Induced Seismicity during Hydraulic Fracturing in HDR Geothermal Exploitation in the Yishu Fault Zone in China. Geofluids **5**, 1-19 (2021).

[11] A. Sattari, D. Eaton, Finite element modelling of fault stress triggering due to hydraulic fracturing. In: GeoConvention 2014: FOCUS adapt, refine, sustain. Calgary (2014).

[12] G. Ding, H. Liu, D. Xia, D. Wang, F. Huang, H. Guo, et al., Experimental Study of the Shear Characteristics of Fault Filled with Different Types of Gouge in Underground Gas Storage. Energies (Basel) 29, **16** (7), 3119 (2023).

[13] A.C.G. Nagelhout, J.P.A. Roest, Investigating fault slip in a model of an underground gas storage facility. International Journal of Rock Mechanics and Mining Sciences **34** (3-4), 212.e1-212.e14. (1997).

[14] P. Xie, H. Wen, G. Wang, An analytical solution of stress distribution around underground gas storage cavern in bedded salt rock. Journal of Renewable and Sustainable Energy **10** (3), 34101 (2018).

[15] T. Wang, C. Yang, J. Chen, J.J.K. Daemen, Geomechanical investigation of roof failure of China's first gas storage salt cavern. Eng. Geol. [Internet]. **243**, 59-69 (2018).
Available from: https://linkinghub.elsevier.com/retrieve/pii/S001379521830200X

[16] J. Kaldi, R. Daniel, E. Tenthorey, K. Michael, U. Schacht, A. Nicol, et al., Containment of CO2 in CCS: Role of Caprocks and Faults. Energy Procedia **37**, 5403-10 (2013).

[17] A. Nicol, H. Seebeck, B. Field, D. McNamara, C. Childs, J. Craig, et al., Fault Permeability and CO2 Storage. Energy Procedia **114**, 3229-36 (2017).

[18] K. Anyim, Q. Gan, Fault zone exploitation in geothermal reservoirs: Production optimization, permeability evolution and induced seismicity. Advances in Geo-Energy Research **1**, 4 (1), 1-12 (2020).

[19] A. Mazzoldi, A. Borgia, M. Ripepe, E. Marchetti, G. Ulivieri, M. della Schiava, et al., Faults strengthening and seismicity induced by geothermal exploitation on a spreading volcano, Mt. Amiata, Italia. Journal of Volcanology and Geothermal Research **301**, 159-68 (2015).

[20] A. Tajduś, M, Cała, K. Tajduś, The influence of normal fault on initial state of stress in rock mass. Studia Geotechnica et Mechanica **38** (1) (2016).

[21] J. Byerlee, Friction of rocks. Pure and Applied Geophysics Pageoph. **116** (4-5), 615-26 (1978).

[22] K. Tajduś, New method for determining the elastic parameters of rock mass layers in the region of underground mining influence. International Journal of Rock Mechanics and Mining Sciences **46** (8), 1296-305 (2009).

[23] Z. Kleczek, Geomechanika górnicza. Śląskie Wydawnictwo Techniczne, Katowice, Poland. 1994.

[24] I.M. Pietuchow, A.M. Linkow, Teorija zaszczitnychpłastow. Izd. Niedra (1976).

[25] E. Grun, Analyse und Prognose von Unstetigkeiten als Folge Bergbaubedinger Bodenbewegungen im linksrheinischen Steinkohlengebiet [PhD Dissertation]. Aachen RWTH. Aachen. RWTH Aachen (1995).